Int. J. Electrochem. Sci., 9 **(2014)** 120 - 138

International Journal of
ELECTROCHEMICAL
SCIENCE
www.electrochemsci.org

Experimental and Theoretical Studies of the Adsorption and Corrosion Inhibition of 6-phenylpyridazine-3(2H)-thione on Carbon Steel in 2.0 M H_3PO_4 solution

D. Ben Hmamou[1], *A. Zarrouk*[2], *R. Salghi*[1,*], *H. Zarrok*[3], *Eno E. Ebenso*[4,*], *B. Hammouti*[2], *M. M. Kabanda*[4], *N. Benchat*[2], *O. Benali*[5]

[1] Laboratory of Environmental Engineering and Biotechnology, ENSA, Université Ibn Zohr, PO Box 1136, 80000 Agadir, Morocco
[2] LCAE-URAC 18, Faculty of Science, University of Mohammed Premier, Po Box 717 60000 Oujda, Morocco
[3]Laboratory Separation Processes, Faculty of Science, University Ibn Tofail PO Box 242, Kenitra, Morocco.
[4]Material Science Innovation & Modelling (MaSIM) Research Focus Area, Faculty of Agriculture, Science and Technology, North-West University (Mafikeng Campus), Private Bag X2046, Mmabatho 2735, South Africa
[5]Départment de Biologie, Faculté des sciences et de la technologie, Université Dr. Tahar Moulay – Saïda- Algeria
[*]E-mail: r.salghi@uiz.ac.ma; Eno.Ebenso@nwu.ac.za

Received: 30 September 2013 / *Accepted:* 27 October 2013 / *Published:* 15 November 2013

The corrosion inhibition efficiency of 6-phenylpyridazine-3(2H)-thione (PPT) for carbon steel in 2.0 M H_3PO_4 has been studied using weight loss, polarization, electrochemical impedance spectroscopy and SEM techniques. The results show that PPT is a good inhibitor in 2.0 M H_3PO_4. Effects of temperature and acid concentration on inhibitive performance were investigated. Polarization curves reveal that PPT acts as a mixed-type inhibitor. The electrochemical impedance spectroscopy showed that the charge transfer resistance increases and the double layer capacitance decreases on increasing pyridazine derivative concentration. Activation energy of corrosion and other thermodynamic parameters such as standard free energy, standard enthalpy, and standard entropy of the adsorption process revealed better and well-ordered physical adsorption mechanism in the presence of PPT. Adsorption isotherms in absence or presence of PPT as inhibitor appropriately fit the Langmuir isotherm. Theoretical investigations have established that the interaction of PPT with the metal steel surface is mainly through the sulphur atom and the π system of the aromatic ring. The molecule···metal surface interactions are strongest in the aqueous acidic solution.

Keywords: carbon steel, corrosion, H_3PO_4, 6-phenylpyridazine-3(2H)-thione, molecular surface interactions.

1. INTRODUCTION

Carbon steel is the major construction material, which is extensively used in most of the major industries particularly in the nuclear, petroleum, power and food production, medical, chemical and electrochemical industries. Carbon steel suffers from certain types of corrosion in some environments. The use of inhibitors is one of the most practical methods for protection against corrosion. The concentration of a given inhibitor needed to protect a metal depends on a number of factors: such as (i) composition of the environment, (ii) temperature, (iii) velocity of the liquid, (iv) the presence or absence in the metal of internal or external stresses, (v) composition of the metal, and (vi) the presence of any other metal content. The influence of organic compounds containing nitrogen on the corrosion of steel in acidic media has been reported [1-14]. These inhibitors are adsorbed on the metal surface and protect the metal surface from the corrosive medium. Adsorption of these compounds on the metal surface depends on: (i) nature and charge of the metal, (ii) the type of electrolyte, and (iii) the chemical structure of the inhibitor.

H_3PO_4 is widely used in the surface treatment of steel such as chemical and electrolytic polishing or etching, chemical colouring, removal of oxide film, phosphating, passivating, and surface cleaning. Although H_3PO_4 is a medium-strong acid, it shows strong corrosiveness on steel. There is a great need to protect steel materials used in H_3PO_4 solution. Comparing with the corrosion inhibition in HCl and H_2SO_4 medium, there are lower attentions in H_3PO_4 medium. Many organic compounds have been used as inhibitors of steel corrosion in H_3PO_4 solution, such as polymers [15], N-heterocyclic compounds [16-19], L-cysteine [20], thiosemicarbazide derivatives [21-23] and ruthenium-ligand complex [24]. However, literature reveals that data regarding the use of pyridazine and its derivatives as corrosion inhibitor for steel in H_3PO_4 are very scarce. 6-phenylpyridazine-3(2H)-thione (PPT) is an ordinary pyridazine derivative with low-cost and good water-solubility (Fig.1). To the best of our knowledge, PPT has not been used as a corrosion inhibitor for steel in H_3PO_4. By considering the remarks mentioned above, in the present work, the inhibition effect of PPT on the corrosion of carbon steel in 2.0 M H_3PO_4 solution at 298-328K was studied using weight loss, potentiodynamic polarisation curves, electrochemical impedance spectroscopy (EIS) and scanning electron microscopy (SEM) methods. The phenomenon of adsorption and adsorption isotherm for PPT on steel surface was determined. Both standard thermodynamic parameters and kinetic parameters were calculated and discussed in detail. A probable inhibitive mechanism is presented from the viewpoint of adsorption. Furthermore, quantum chemical study using density functional theory (DFT) at the BLYP/6-31G(d,p) method and molecular dynamics (MD) simulations were employed in an attempt to gain insights into the reactive site of the compound and its mechanism of adsorption on the steel surface *in vacuo*, in pure water solution and aqueous acidic solution. The study *in vacuo* is considered as a preliminary step towards other studies (i.e., it provides information which can serve as input for studies in other medium). Studies in the water solution (bulk solvent consideration) and presence of a solvent is meant to mimic the situation found in most electrochemical environment and the study in the solution of PO_4^{3-} ions is meant to simulate the situation in a H_3PO_4 acidic medium.

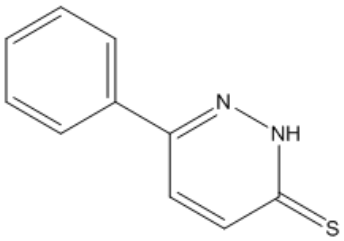

Figure. 1. Molecular structure of 6-phenylpyridazine-3(2H)-thione (**PPT)**

2. EXPERIMENTAL METHODS

2.1. Materials

The steel used in this study is carbon steel (Euronorm: C35E carbon steel and US specification: SAE 1035) with a chemical composition (in wt%) of 0.370 % C, 0.230 % Si, 0.680 % Mn, 0.016 % S, 0.077 % Cr, 0.011 % Ti, 0.059 % Ni, 0.009 % Co, 0.160 % Cu and the remainder iron (Fe). The carbon steel samples were pre-treated prior to the experiments by grinding with emery paper SiC (120, 600 and 1200); rinsed with distilled water, degreased in acetone in an ultrasonic bath immersion for 5 min, washed again with bidistilled water and then dried at room temperature before use. The acid solution (2.0 M H_3PO_4) was prepared by dilution of an analytical reagent grade 85% H_3PO_4 with double-distilled water. The concentration range of PPT employed was 10^{-7} M to 10^{-4} M.

2.2. Methods

2.2.1. Weight loss measurements

Gravimetric measurements were carried out at definite time interval of 2 h at room temperature using an analytical balance (precision ± 0.1 mg). The carbon steel specimens used have a rectangular form (length = 1.6 cm, width = 1.6 cm, thickness = 0.07 cm). Gravimetric experiments were carried out in a double glass cell equipped with a thermostated cooling condenser containing 80 mL of non-de-aerated test solution. After immersion period, the steel specimens were withdrawn, carefully rinsed with bidistilled water, ultrasonic cleaning in acetone, dried at room temperature and then weighed. Triplicate experiments were performed in each case and the mean value of the weight loss was calculated.

2.2.2. Electrochemical measurements

Electrochemical experiments were conducted using impedance equipment (Tacussel-Radiometer PGZ 100) and controlled with Tacussel corrosion analysis software model Voltamaster 4. A conventional three-electrode cylindrical Pyrex glass cell was used. The temperature was thermostatically controlled. The working electrode was carbon steel with the surface area of 1 cm^2. A

saturated calomel electrode (SCE) was used as a reference. All potentials were given with reference to this electrode. The counter electrode was a platinum plate of surface area of 1 cm^2. A saturated calomel electrode (SCE) was used as the reference; a platinum electrode was used as the counter-electrode. All potentials are reported *vs*. SCE. All electrochemical tests have been performed in aerated solutions at 298 K.

For polarization curves, the working electrode was immersed in a test solution during 30 min until a steady state open circuit potential (E_{ocp}) was obtained. The polarization curve was recorded from -800 to -200 mV/SCE with a scan rate of 1 mV s^{-1}. AC impedance measurements were carried-out in the frequency range of 100 kHz to 10 mHz, with 10 points per decade, at the rest potential, after 30 min of acid immersion, by applying 10 mV ac voltage peak-to-peak. Nyquist plots were made from these experiments. The best semicircle was fit through the data points in the Nyquist plot using a non-linear least square fit so as to give the intersections with the *x*-axis.

2.2.3. Scanning electron microscopy (SEM)

Immersion corrosion analysis of steel samples in the acidic solutions with and without the optimal concentration of the inhibitor was performed using SEM. Immediately after the corrosion tests, the samples were subjected to SEM studies to know the surface morphology using SEM Jeol JSM-5800 scanning electron microscope.

2.2.4. Computational Details

Geometry optimization was performed using density functional theory (DFT). The Becke's Three Parameter Hybrid Functional using the Lee-Yang-Parr correlation functional theory was selected for the calculations. Calculations were done using the 6-31+G(d) basis set. The Molecular properties estimated include the highest occupied molecular orbital (HOMO), lowest unoccupied molecular orbital (LUMO) and other molecular properties derived from HOMO and LUMO and their respective energies.

All optimization calculations were done using the Spartan 10 V1.01 program (Materials studio). Schematic structures were drawn using the ChemOffice package in the UltraChem 2010 version while optimized structures were drawn using the Spartan 10 V1.01 program.

The molecular dynamics simulations were performed utilizing the Amorphous Cell, the Build Layer and the Discover Modules in Materials studio 6.0 program [25-28].

The iron surface as cleaved to a Fe (110) surface and then minimizer procedure in cooperated in Discover Module. The isolated PPT molecule was then build and optimized to determine the lowest energy structure. Using Amorphous Cell, the compound was constructed in a periodic box. The compound, in the periodic box, was then mounted onto the metal surfaces by using the Build Layer section in Materials Studio. The vacuum slab with 30 Å thicknesses was built to separate the compound from the metal surface. The Molecular Dynamics simulation was performed under 298 K, NVT ensemble, with a time step of 0.1 fs and simulation time of 0.5 ps. The PCFF forcefield was

utilized to generate the forcefields for the different atom types. The binding energy on the metal surface was estimated following the equation:

$$E_{binding} = E_{total} - (E_{surface} + E_{inhibitor}) \quad (1)$$

where E_{total} is the total energy of the surface and inhibitor, $E_{surface}$ is the energy of the surface without the inhibitor, and $E_{inhibitor}$ is the energy of the inhibitor without the surface. Similar procedures were followed for the estimation of the binding energy in pure water solution and in the H_3PO_4 acidic solution. Studies have shown that the adsorption energy of the inhibitors on the metal surface correlates with the inhibition efficiency exhibited by the inhibitor [29].

3. RESULTS AND DISCUSSION

3.1. Polarization curves

The potentiodynamic polarization curves of carbon steel in 2.0 M H_3PO_4 solution in the absence and presence of 6-phenylpyridazine-3(2H)-thione (PPT) are shown in Fig. 2. The values of related electrochemical parameters i.e., corrosion potential (E_{corr}), corrosion current density (i_{corr}), cathodic Tafel slope (b_c) and inhibition efficiency η_p were calculated and given in Table 1. The η_p was calculated from polarization measurements according to the relation given below;

$$\eta_p = \left(\frac{i_{corr(uninh)} - i_{corr(inh)}}{i_{corr(uninh)}} \right) \times 100 \quad (2)$$

where $i_{corr(uninh)}$ and $i_{corr(inh)}$ are uninhibited and inhibited corrosion current densities, respectively. Corrosion current densities were obtained by the extrapolation of the current potential lines to the corresponding corrosion potentials. Herein, the corrosion rates were calculated assuming that the whole surface of steel is attacked by corrosion and no local corrosion is observed. As it can be clearly seen from Fig. 2, the addition of inhibitor to the corrosive solution both reduces anodic dissolution of iron and also retards cathodic hydrogen evolution reactions as would be expected. This may be ascribed to adsorption of the inhibitor molecules over the steel surface. The presence of the inhibitor (PPT) does not remarkably shift the corrosion potential (E_{corr}), while the cathodic Tafel slopes does not change with the increase concentration of PPT. According to Riggs [30], the classification of a compound as an anodic or cathodic type inhibitor is feasible when the OCP displacement is at least 85 mV in relation to that one measured for the blank solution. Therefore, PPT can be classified as a mixed type inhibitor in H_3PO_4 solution. The parallel cathodic Tafel lines (Fig. 2) suggests that the addition of the inhibitor to the 2.0 M H_3PO_4 solution does not modify the hydrogen evolution mechanism and the reduction of H^+ ions at the steel surface which occurs mainly through a charge transfer mechanism [31].

Table 1. Electrochemical parameters of carbon steel at various concentrations of PPT in 2.0 M H_3PO_4 and corresponding inhibition efficiency.

Inhibitor	Conc.(M)	E_{corr} (mV/SCE)	I_{corr} (μA/cm^2)	-b_c (mV/dec)	η_p (%)
Blank	2.00	-488	2718	135	----
PPT	10^{-4}	-447	112	143	95.8
	10^{-5}	-449	240	139	91.2
	10^{-6}	-524	520	141	80.9
	10^{-7}	-504	878	146	67.7

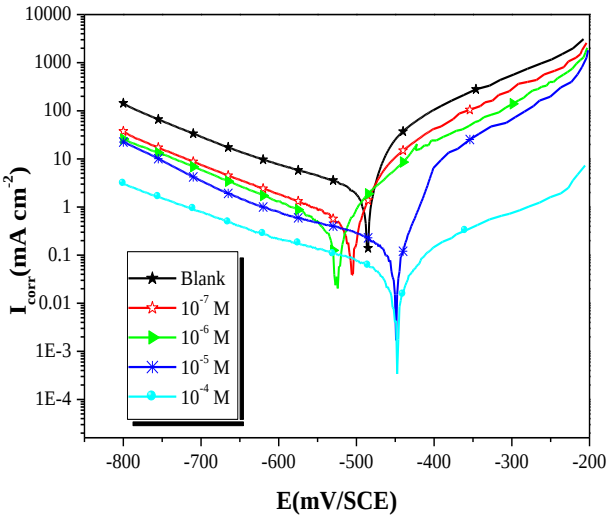

Figure 2. Potentiodynamic polarization curves of carbon steel in 2.0 M H_3PO_4 in the presence of different concentrations of PPT.

3.2. Electrochemical impedance spectroscopy measurements

Fig. 3 shows the Nyquist diagrams of carbon steel in 2.0 M H_3PO_4 solutions containing different concentrations of PPT at 298K. All the impedance spectra exhibit one single depressed semicircle. The diameter of semicircle increases with the increase of PPT concentration and the decrease of the temperature. The semicircular appearance shows that the corrosion of carbon steel is controlled by the charge transfer and the presence of PPT does not change the mechanism of carbon steel dissolution [32]. In addition, these Nyquist diagrams are not perfect semicircles. The deviation of semicircles from perfect circular shape is often referred to as the frequency dispersion of interfacial impedance [32, 33]. This behavior is usually attributed to the inhomogeneity of the metal surface arising from surface roughness or interfacial phenomena [34, 35] which is typical for solid metal electrodes. Generally, when a non-ideal frequency response is present, it is commonly accepted to employ the distributed circuit elements in the equivalent circuits. What is most widely used is the constant phase element (CPE), which has a non-integer power dependence on the frequency [36, 37]. Thus, the equivalent circuit depicted in Fig. 4 is employed to analyze the impedance spectra, where R_s

represents the solution resistance, R_t denotes the charge-transfer resistance, and a CPE instead of a pure capacitor represents the interfacial capacitance. Excellent fit with this model was obtained for all experimental data. As an example, the Nyquist plots of both experimental and simulated data of carbon steel in 2.0 M H_3PO_4 solution containing 10^{-7} M of PPT are shown in Fig. 5. The impedance of a CPE is described by the expression:

$$Z_{CPE} = \frac{1}{Y_0 (j\omega)^n} \quad (3)$$

where Y_0 is the magnitude of the CPE, ω is the angular frequency at which -Z reaches its maximum values and n is the deviation parameter of the CPE: $-1 \leq n \leq 1$. The values of the interfacial capacitance C_{dl} can be calculated from CPE parameter values Y_0 and n using the expression [38]:

$$C_{dl} = \frac{Y_0 \omega^{n-1}}{\sin(n\pi/2)} \quad (4)$$

Table 2. Electrochemical Impedance parameters for corrosion of carbon steel in acid medium at various contents of PPT.

	Conc. (M)	R_s (Ω cm^2)	R_{ct} (Ω cm^2)	n	CPE-T/Y_0 ×10^{-5} (s^n/Ω cm^2)	C_{dl} (μF/cm^2)	η_i (%)
Blank	2.0	1.20	14.00	0.88	21.024	94.96	-----
PPT	10^{-4}	1.25	303.7	0.76	7.2416	21.69	95.4
	10^{-5}	1.20	86.77	0.86	6.3304	27.13	83.9
	10^{-6}	1.15	57.88	0.86	7.3423	30.18	75.8
	10^{-7}	1.18	40.24	0.90	7.9043	41.72	65.2

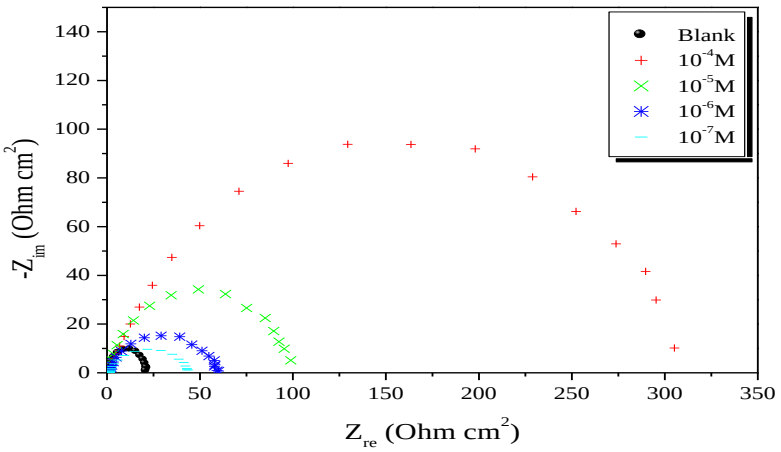

Figure 3. Nyquist diagrams of carbon steel with different concentrations of PPT at 298K.

The values of percentage inhibition efficiency η_i were calculated from the values of R_{ct} according to the following equation [16]:

$$\eta_i = \left(\frac{R_{ct(inh)} - R_{ct(uninh)}}{R_{ct(inh)}} \right) \times 100 \qquad (5)$$

where $R_{ct(inh)}$ and $R_{ct(uninh)}$ are the charge-transfer resistance values with and without inhibitor, respectively. The values of the parameters such as R_s, R_{ct}, Y_0, n through EIS fitting as well as the derived parameters C_{dl} and η_i % are listed in Table 2.

As is seen from Table 2, the C_{dl} values decrease with the increase of PPT concentration, which suggests that PPT functions by adsorption on the carbon steel surface. It is inferred that the PPT molecules gradually replace the water molecules by adsorption at the metal/solution interface, which leads to the formation of a protective film on the carbon steel surface and thus decreases the extent of the dissolution reaction [33]. Moreover, the increase of PPT concentration leads to the increase of R_{ct} and η_i% values. The corrosion inhibition efficiency reaches more than 95% in the presence of 10^{-4} M PPT. The change trend of η_i % can be related to the surface coverage of PPT on carbon steel, namely, with an increase in PPT concentration, its surface coverage on carbon steel also increases. The high η_i% (and surface coverage) at the low concentration of PPT leads to the assumption that the adsorption of PPT molecules occurs not on the whole surface of carbon steel, but only on the active sites.

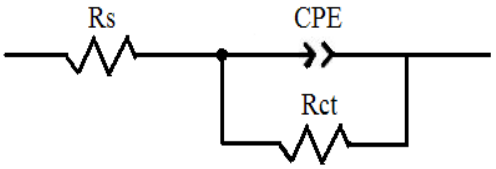

Figure. 4. The electrochemical equivalent circuit used to fit the impedance spectra.

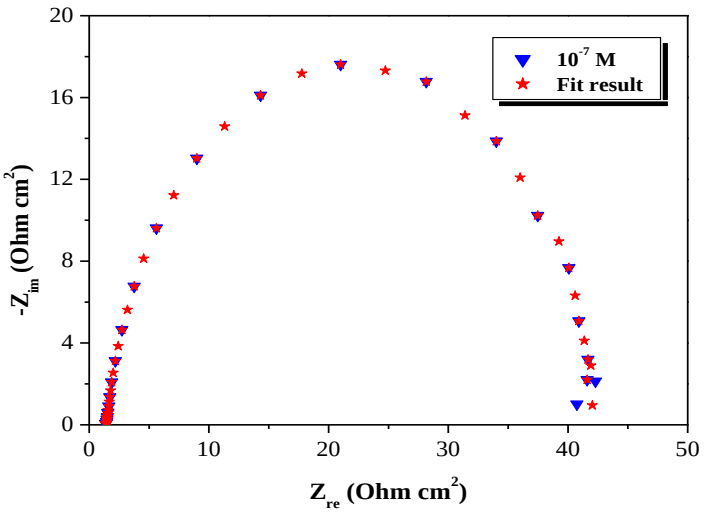

Figure 5. Curve fitting of EIS data of carbon steel in 2.0 M H_3PO_4 with 10^{-7} M of PPT to Nyquist plots at E_{corr}.

3.3. Weight loss, corrosion rates and inhibition efficiency

The corrosion rate (A) of carbon steel specimens after 2 h exposure to 2.0 M H_3PO_4 solution with and without the addition of various concentrations of the investigated inhibitor was calculated and the obtained data are listed in Table 3. The variation of A with inhibitor concentrations is shown in Fig. 6. The corrosion rate, A (mg cm^{-2} h^{-1}), surface coverage (θ) and inhibition efficiency η_w of each concentration were calculated using the following equations [39]:

$$A = \frac{\Delta W}{St} \quad (6)$$

$$\theta = \frac{A_{uninh} - A_{inh}}{A_{uninh}} \quad (7)$$

$$\eta_w = \left(\frac{A_{uninh} - A_{inh}}{A_{uninh}} \right) \times 100 \quad (8)$$

where ΔW is the average weight loss (mg), S is the surface area of specimens (cm^2), and t is the immersion time (h), A_{uninh} and A_{inh} are corrosion rates in the absence and presence of inhibitor, respectively.

Table 3. Effect of PPT concentration on corrosion data of carbon steel in 2.0 M H_3PO_4

Inhibitor	Conc. (M)	A (mg cm^{-2} h^{-1})	η_w (%)	Θ
Blank	2.0	1.972	------	------
PPT	10^{-4}	0.070	96.4	0.964
	10^{-5}	0.188	90.4	0.904
	10^{-6}	0.457	76.8	0.768
	10^{-7}	0.618	68.6	0.686

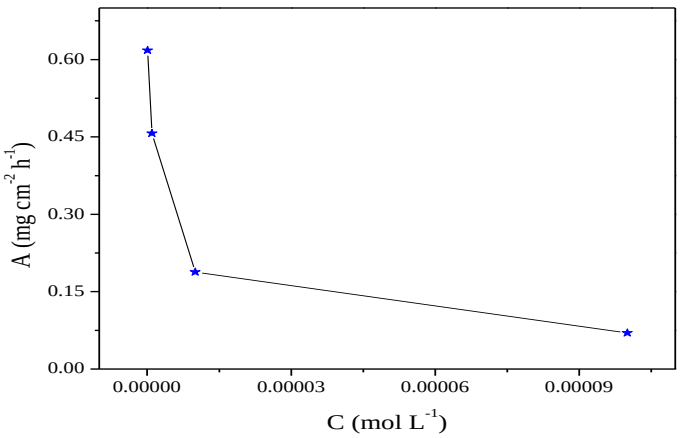

Figure 6. Relationship between the corrosion rate and inhibitor concentration for carbon steel after 2 h immersion in 2.0 M H_3PO_4 at 298K.

It is clear that η_w increased with increasing inhibitor concentration, while corrosion rate decreased. This could be due to the fact that the inhibitor molecules act by adsorption on the metal

surface [40]. The variation of η_w and inhibitor concentrations in 2.0 M H_3PO_4 solution at 298 K is shown in Fig 7. The maximum η_w value of (10^{-4} M) of this inhibitor was found.

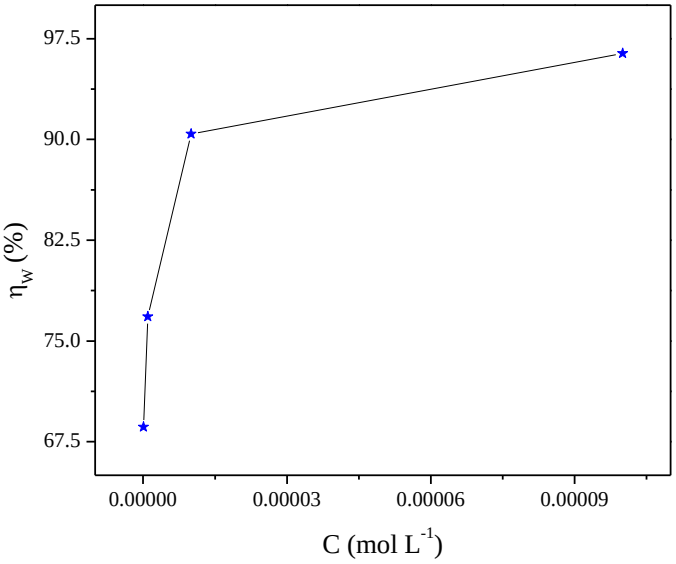

Figure 7. Relationship between the inhibition efficiency and inhibitor concentration for carbon steel after 2 h immersion in 2.0 M H_3PO_4 at 298K.

3.3.1. Effect of temperature

Fig. 8 and 9, show the Tafel plots of carbon steel in 2.0 M H_3PO_4 in absence and presence of 10^{-4} M PPT in temperature range 298-328K. Effect of temperature has been studied in order to determine the activation energy of the corrosion process and the thermodynamics of adsorption of PPT on carbon steel surface. Data in Table 4 shows that by increasing the temperature the corrosion rate increases in the absence and presence of PPT. Also, the corrosion rate increases rapidly in absence of PPT, but on addition of PPT, the corrosion rate rapidly decrease i.e. PPT is an efficient inhibitor in the temperature range 298-328K and the values of inhibition efficiency is almost constant in the temperature range 318-328K.

The activation parameters were calculated from the Arrhenius-type plot according to equation:

$$I_{corr} = k \exp\left(-\frac{E_a}{RT}\right) \quad (9)$$

where E_a is the apparent activation corrosion energy, R is the universal gas constant and k is the Arrhenius pre-exponential constant Arrhenius plots for the corrosion density of carbon steel in the case of PPT are given in Fig. 10. Values of apparent activation energy of corrosion (E_a) for carbon steel in 2.0 M H_3PO_4 with the absence and presence of pyridazine derivative were determined from the slope of Ln (I_{corr}) versus 1/T plots and shown in Table 5.

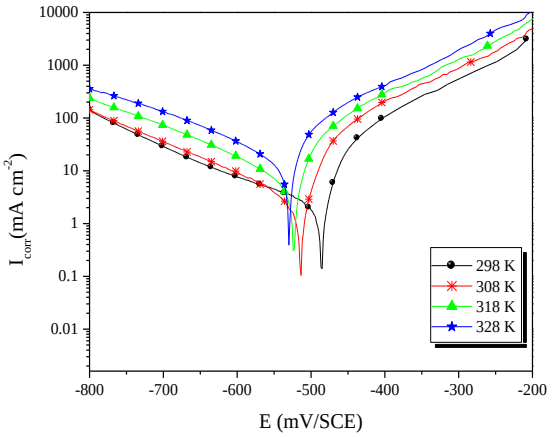

Figure 8. Potentiodynamic polarisation curves of carbon steel in 2M H_3PO_4 at different temperatures.

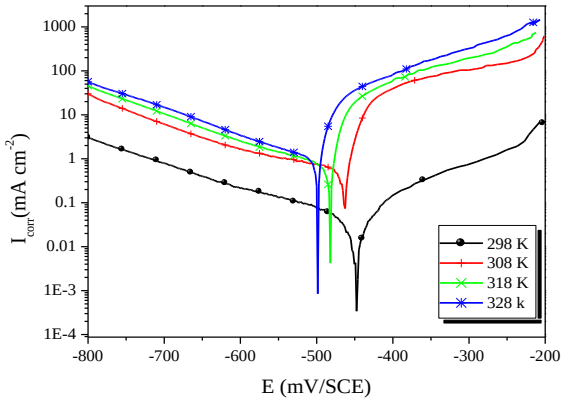

Figure 9. Potentiodynamic polarisation curves of carbon steel in 2M H_3PO_4 in the presence of 10^{-4} M of PPT at different temperatures.

Table 4. Various corrosion parameters for carbon steel in 2M H_3PO_4 in absence and presence of optimum concentration of PPT at different temperatures.

Inhibitor	Temp (K)	E_{corr} (mV/SCE)	I_{corr} (µA cm^{-2})	$-b_c$ (mV/dec)	η_p (%)
Blank	298	-488	2718	135	----
	308	-532	4220	137	----
	318	-523	6610	132	----
	328	-514	11890	139	----
PPT	298	-447	112.6	143	95.8
	308	-496	260.7	147	93.8
	318	-480	553.6	145	91.6
	328	-496	1061	142	91.1

According to the report in literature [40, 41], higher value of E_a was considered as physical adsorption that occurred in the first stage. Because the electrochemical corrosion is relevant to heterogeneous reactions, the preexponential factor A in the Arrhenius equation is related to the number of active centers. There are two possibilities about these active centers with different E_a on the metal

surface: (1) the activation energy in the presence of inhibitors is lower than that of pure acidic medium, namely E_a(-inh) < E_a(HCl), which suggests a smaller number of more active sites remain uncovered in the corrosion process; (2) the activation energy in the presence of inhibitor is higher than that of pure acidic medium, E_a(inh) > E_a(HCl), which represents the inhibitor adsorbed on most active adsorption sites (having the lowest energy) and the corrosion takes place chiefly on the active sites (having higher energy).

The data in Table 5 specifically indicate that the value of E_a in the presence of PPT is larger than that in the absence of PPT. Thus, it is clear that the adsorption of PPT on carbon steel surface blocks the active sites from acid solution and consequently increases the apparent activation energy. Then, it can be suggested that the PPT adsorb by physisorption mechanism on the metallic surface.

Table 5. The values of activation parameters E_a, ΔH_a and ΔS_a for carbon steel in 2.0 M H_3PO_4 in the absence and presence of 10^{-4} M of PPT.

Inhibitor	E_a (kJ/mol)	ΔH_a (kJ/mol)	ΔS_a (J/mol K)
Blank	39.50	36.91	-112.98
PPT	60.83	58.24	-67.31

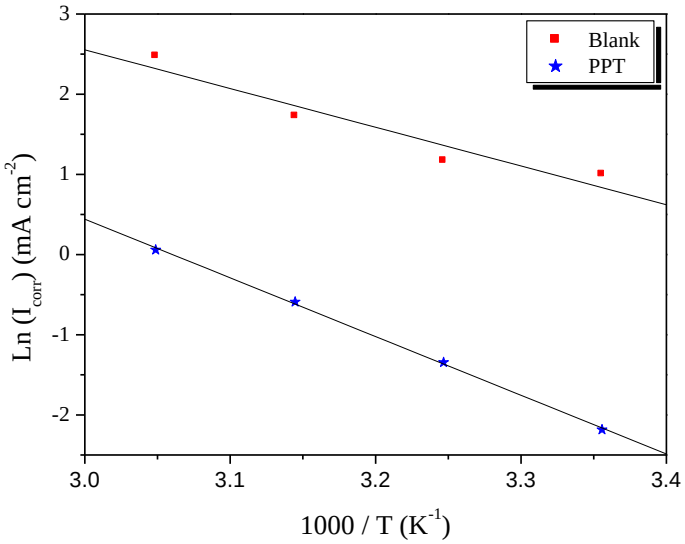

Figure. 10. Arrhenius plots of carbon steel in 2.0 M H_3PO_4 with and without 10^{-4} M of PPT.

Activation parameters like enthalpy (ΔH_a) and entropy (ΔS_a) for the dissolution of carbon steel in 2.0 M H_3PO_4 in the absence and presence of 10^{-4} M PPT were calculated from the transition state equation (Eq. (9)) [42]:

$$i_{corr} = \frac{RT}{Nh}\exp\left(\frac{\Delta S_a}{R}\right)\exp\left(-\frac{\Delta H_a}{RT}\right) \quad (10)$$

where i_{corr} is the corrosion rate, A is the pre-exponential factor, h is Planck's constant, N is the Avogadro number, R is the universal gas constant, ΔH_a is the enthalpy of activation and ΔS_a is the entropy of activation.

Fig. 11 shows that the Arrhenius plots of Ln (i_{corr}/T) versus 1/T gave straight lines with slope ($-\Delta H_a/R$) and intercept (Ln R/Nh + $\Delta S_a/R$) from where ΔH_a and ΔS_a values were calculated. The activation parameters are given in Table 5.

The positive sign of the enthalpies (ΔH_a) reflects the endothermic nature of the steel dissolution process whereas large negative values of entropies (ΔS_a) from PPT imply that the activated complex in the rate determining step represents an association rather than a dissociation step, meaning that a decrease in disordering takes place on going from reactants to the activated complex [43].

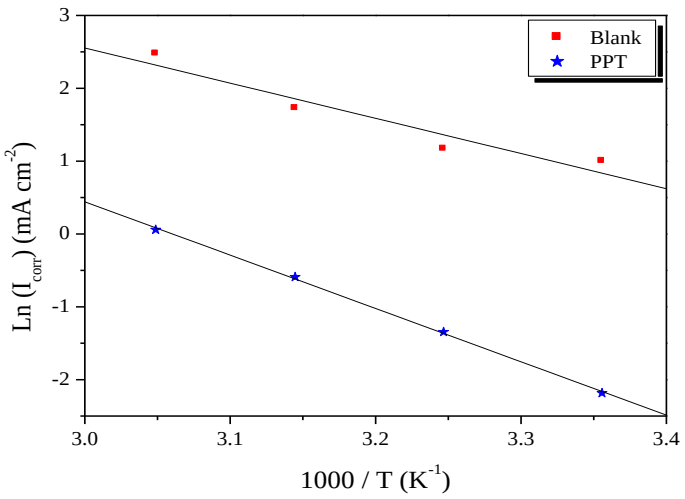

Figure. 11. Arrhenius plots of carbon steel in 2.0 M H_3PO_4 with and without 10^{-4} M of PPT.

3.3.2. Adsorption isotherm and standard adsorption free energy

Corrosion inhibition by organic compounds is mainly due to their ability to adsorb onto a metal surface to form a protective film. The adsorption of organic inhibitors at the metal/solution interface takes place through the replacement of water molecules by organic inhibitor molecules according to following process;

$$Org_{(sol)} + \chi H_2O_{(ads)} \leftrightarrow Org_{(ads)} + \chi H_2O_{(sol)} \quad (11)$$

where $Org_{(sol)}$ and $Org_{(ads)}$ are organic molecules in the solution and adsorbed on the metal surface, respectively, x is the number of water molecules replaced by the organic molecules. It is essential to know the mode of adsorption and the adsorption isotherm that can give valuable information on the interaction of inhibitor and metal surface[56]. Values of surface coverage (θ) corresponding to different concentrations of PPT calculated using the weight loss results at 298 K after 2 h of immersion were used to determine which isotherm best described the adsorption process. The results obtained for the investigated inhibitors in 2.0 M H_3PO_4 solution were tested with several

adsorption isotherms. However, the best fit to the experimental data was obtained with the Langmuir adsorption isotherm equation as follows [44]:

$$\frac{C_{inh}}{\theta} = \frac{1}{K_{ads}} + C_{inh} \quad (12)$$

where C_{inh} is the concentration of inhibitor and K_{ads} the adsorptive equilibrium constant. Langmuir's isotherm assumes that there is no interaction between the adsorbed molecules, the energy of adsorption is independent on the θ, the solid surface contains a fixed number of adsorption sites, and each site holds one adsorbed species. Plots of C_{inh} / θ against C_{inh} yielded straight lines as shown in Fig. 12, and the linear regression parameters are listed in Table 5. Both linear correlation coefficient (R^2) and slope are very close to 1, indicating the adsorption of the investigated inhibitors on steel surface obeys the Langmuir adsorption isotherm in 2.0 M H_3PO_4 solution. The adsorptive equilibrium constant (K_{ads}) can be calculated from the reciprocal of intercept of C_{inh} / θ -C_{inh} curve. K_{ads} is related to the standard free energy of adsorption (ΔG°_{ads}) as shown the following equation [45]:

$$K_{ads} = (\frac{1}{55.5}) \exp(-\frac{\Delta G^{\circ}_{ads}}{RT}) \quad (13)$$

Where R is gas constant and T is absolute temperature of experiment and the constant value of 55.5 is the concentration of water in solution in mol dm^{-3}.

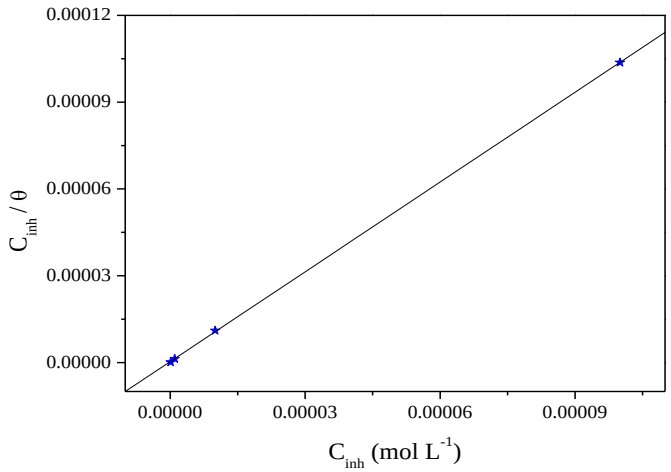

Figure 12. Adsorption isotherm according to Langmuir's model derived from weight loss measurement.

Table 5. Thermodynamic parameters for the adsorption of PPT in 2.0 M H_3PO_4on the carbon steel at 298K.

Slope	K_{ads} (M^{-1})	R^2	ΔG°_{ads} (kJ/mol)
1.03	3.034×10^6	0.999	- 46.90

From Table 5, the negative values of standard free energy of adsorption indicate spontaneous adsorption of organic molecules on metallic surface and also the strong interaction between inhibitor molecules and carbon steel surface [46, 47]. Generally, the standard free energy values of - 20 kJ mol^{-1} or less negative are associated with an electrostatic interaction between charged molecules and charged metal surface (physical adsorption); those of - 40 kJ mol^{-1} or more negative involves charge sharing or transfer from the inhibitor molecules to the metal surface to form a co-ordinate covalent bond (chemical adsorption) [48,49]. Based on the literature[63], the calculated ΔG^{o}_{ads} value in this work indicates that the adsorption mechanism of PPT on carbon steel is chemisorption.

3.4. Surface examination by SEM

Fig. 13 (left and right) shows the SEM images of the carbon steel surface after immersion in 2.0 M H_3PO_4, for a period of 6 h, in absence (left) and presence (right) of 10^{-4} M of PPT, respectively.

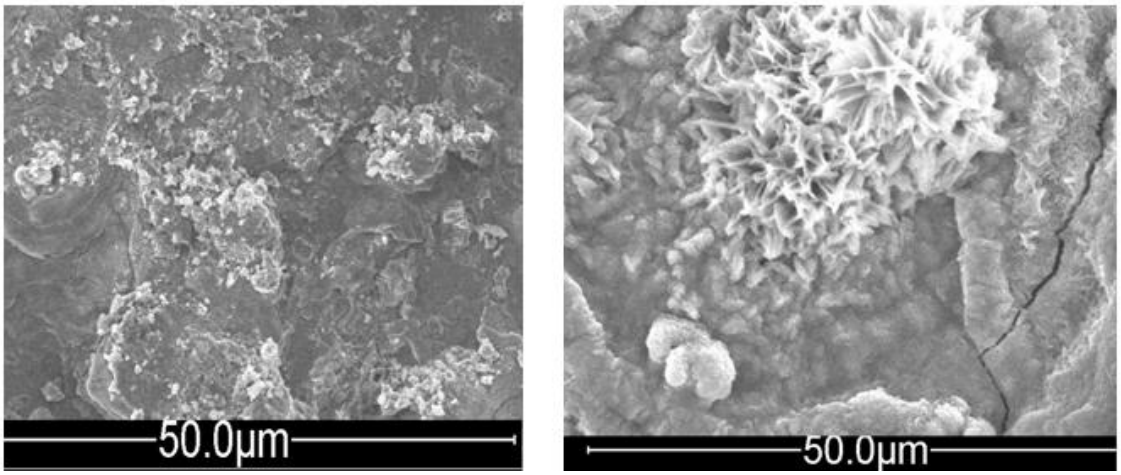

Figure 13. SEM (×2000) images of carbon steel surface after 6 h immersion in 2.0 M H_3PO_4 solution in the (left) absence and (right) presence of 10^{-4} M of PPT.

The SEM micrographs show that the surface of carbon steel is highly damaged in the uninhibited solution (Fig. 13 (left)). However, a smoother surface is seen in the presence of the inhibitor (Fig. 13 (right)). These results indicate that the inhibitor molecules hinder the dissolution of carbon steel by formation of a protective film on the steel surface.

3.5. Computational studies

3.5.1. Optimized structure and related molecular reactivity parameters

The optimized structure and the corresponding highest occupied molecular orbital (HOMO) and the lowest unoccupied molecular orbital (LUMO) are shown in Fig. 14. The HOMO and the

LUMO are interesting to investigate because they provide an idea of the regions on the molecule with the tendency to donate or accept electrons. In PPT, the HOMO density is largely localized on the sulphur atom while the LUMO density is largely on the pyridazine ring. The charges on the atoms provide information on the reactivity sites. The highest negative charge is on the N atom of the NH group and on S atom. This indicates that these are the atoms on which the electrophilic attach would preferably occur. However, since the N atom is already saturated, indicating that the atom with the highest tendency to interact with the metal surface is the S atom, which agrees with the analysis of the HOMO.

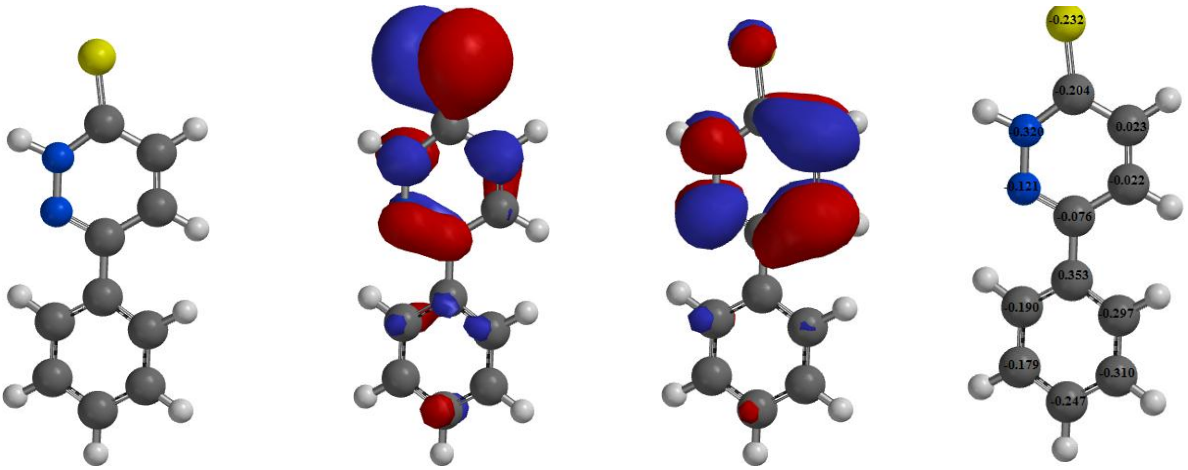

Figure. 14. Optimized structure, HOMO, LUMO and charges on the atoms of PPT

3.5.2. Results of molecular dynamics simulation

Molecular dynamics simulation was performed on Fe (110) *in vacuo*, in water solution and in the presence of PO_4^{3-} ions. The geometry of the resulting simulations and the binding energies of the inhibitor are shown in Fig. 15. *In vacuo*, the PPT atoms are 3.0–3.6 Å from the surface of the metal. The closes part of the PPT is the atoms of the benzene ring (3.0–3.4Å), indicating that the aromatic π system has a greater role in the interaction with the metal surface. The interaction energy has value of −14.05 kcal/mol. The adsorption of PPT on the metal surface therefore results in the lowering of the energy. In pure water solvent, PPT interacts with both the metal surface (from below) and the water molecules (from above). The distance between the N atom and the nearest water molecule is 2.9 Å while the distance between the nearest water molecule and the S atom is 2.588Å. The water molecules also form π···H–O type of interactions with the aromatic π system of the benzene ring. The interaction energy in water solution is nearly 8 times the interaction of PPT with the metal surface *in vacuo*. The results therefore suggest that the water molecules form strong bonds with the PPT molecule.

In acidic solution containing some anions, such as chloride, sulfate or phosphate ions, adsorption of organic molecules is not always a direct combination of the molecule with the metal surface [50]. Some anions tend to get adsorbed on the metal surface, and therefore interfere with the adsorption of the organic molecule on the metal surface. In some cases, the adsorption of organic

molecules can occur through the already adsorbed chloride or sulfate ions, which interfere with the adsorbed organic molecules [50]. In the simulation of the interaction of PPT with Fe (110) surface in the presence of phosphate ions, it has been observed that some phosphate ions interact directly with the metal surface. The calculated interaction energy of PPT with the Fe (110) surface in acidic medium is nearly 9 times the interaction of Fe with pure water solvent. This large value of the interaction energy suggests that the binding energy between PPT on the metal surface is very high, indicating that PPT would have a strong tendency to protect steel surface from corrosion.

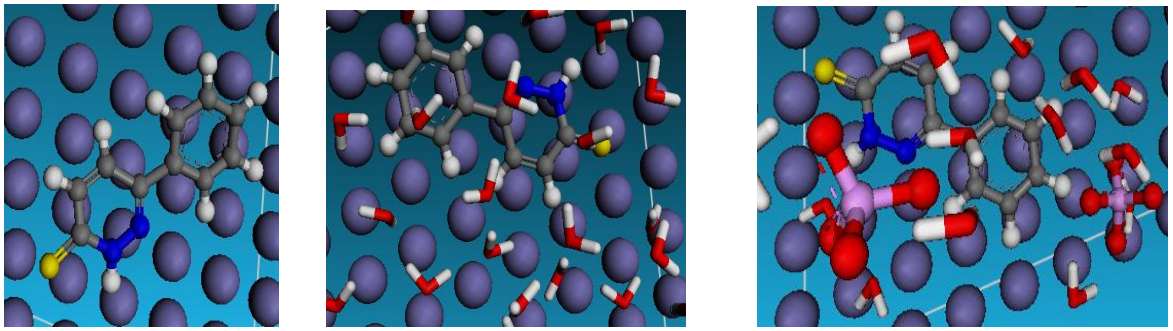

(a) −14.05 kcal/mol (b) −112.18 kcal/mol (c) −959.30 kcal/mol

Figure 15. Adsorption configurations of Metronidazole (PPT) on the Fe (110): (a) Fe + PPT (b) Fe + PPT+H_2O (c) Fe + PPT + H_2O + PO_4^{3-}. The binding energies (kcal/mol) reported below each adsorption configuration.

4. CONCLUSIONS

6-phenylpyridazine-3(2H)-thione (PPT) has proved to be good inhibitor for the corrosion of carbon steel in phosphoric acid. This inhibitor acts as mixed type inhibitor. η% was found to increase with increase in concentration of inhibitor. Data obtained from ac impedance technique show a frequency distribution and therefore a modeling element with frequency dispersion behavior with the use of a constant phase element (CPE). The calculated from EIS show the same trend as those estimated from polarization and weight loss measurements. The inhibition of carbon steel in phosphoric acid was found to obey Langmuir adsorption isotherm. The negative values of ΔG^{o}_{ads} indicate spontaneous adsorption of the inhibitor on the surface of steel. Kinetic parameters are calculated and discussed in detail. Surface morphological studies using SEM analysis showed that the inhibitor molecules form a good protective film on the steel surface. Quantum chemical studies and molecular dynamic studies have shown that the regions with the highest tendency to donate electrons to the metal surface are the S atom and the aromatic ring of the molecule. The molecular surface interactions, estimated using molecular dynamics, suggest that PPT bind strongest in the presence of aqueous acidic medium and bind the least *in vacuo*. In this way, all approaches utilized for the study have demonstrated the ability of PPT molecule to protect steel metal surface in the presence of acidic medium.

References

1. H. Zarrok, A. Zarrouk, R. Salghi, Y. Ramli, B. Hammouti, M. Assouag, E. M. Essassi, H. Oudda, M. Taleb, *J. Chem. Pharm. Res*. 4 (2012) 5048.
2. H. Zarrok, H. Oudda, A. El Midaoui, A. Zarrouk, B. Hammouti, M. Ebn Touhami, A. Attayibat, S. Radi, R. Touzani, *Res. Chem. Intermed*., (2012) DOI: 10.1007/s11164-012-0525-x.
3. H. Zarrok, A. Zarrouk, R. Salghi, H. Oudda, B. Hammouti, M. Assouag, M. Taleb, M. Ebn Touhami, M. Bouachrine, S. Boukhris, *J. Chem. Pharm. Res*. 4, (2012) 5056.
4. A. Zarrouk, M. Messali, M. R. Aouad, M. Assouag, H. Zarrok, R. Salghi, B. Hammouti, A. Chetouani, *J. Chem. Pharm. Res*. 4 (2012) 3427.
5. H. Zarrok, A. Zarrouk, B. Hammouti, R. Salghi, C. Jama, F. Bentiss, *Corros. Sci*. 64 (2012) 243.
6. H. Bendaha, A. Zarrouk, A. Aouniti, B. Hammouti, S. El Kadiri, R. Salghi, R. Touzani, *Phys. Chem. News*, 64 (2012) 95.
7. M. Elbakri, R. Touir, M. Ebn Touhami, A. Zarrouk, Y. Aouine, M. Sfaira, M. Bouachrine, A. Alami, A. El Hallaoui, *Res. Chem. Intermed*., (2012) DOI: 10.1007/s11164-012-0768-6.
8. A. Ghazoui, R. Saddik, B. Hammouti, A. Zarrouk, N. Benchat, M. Guenbour, S. S. Al-Deyab, I. Warad, *Res. Chem. Intermed*., (2012) DOI: 10.1007/s11164-012-0763-y.
9. D. Ben Hmamou, R. Salghi, A. Zarrouk, M. Messali, H. Zarrok, M. Errami, B. Hammouti, Lh. Bazzi , A. Chakir, *Der Pharm. Chem*. 4 (2012) 1496.
10. H. Zarrok, R. Salghi, A. Zarrouk, B. Hammouti, H. Oudda, Lh. Bazzi, L. Bammou, S. S. Al-Deyab, *Der Pharm. Chem*. 4 407 (2012) 416.
11. A. Ghazoui, R. Saddik, N. Benchat, B. Hammouti, M. Guenbour, A. Zarrouk, M. Ramdani, *Der Pharm. Chem*. 4 (2012) 352
12. H. Zarrok, R. Saddik, H. Oudda, B. Hammouti, A. El Midaoui, A. Zarrouk, N. Benchat, M. Ebn Touhami, *Der Pharm. Chem*. 3 (2011) 272.
13. Y. Jianguo, W. Lin, V. Otieno-Alego, D. P. Schweinsberg, *Corros. Sci.* 37 (1995) 975.
14. L. Wang, *Corros. Sci.* 43 (2001) 2281.
15. L. Wang, *Corros. Sci.* 48 (2006) 608.
16. X.H. Li, S.D. Deng, H. Fu, *Mater. Chem. Phys*. 115 (2009) 815.
17. X.H. Li, S.D. Deng, H. Fu, *Corros. Sci.* 53 (2011) 3704.
18. X.H. Li, S.D. Deng, H. Fu, *Corros. Sci.* 53 (2011) 664.
19. H. Zarrok, A. Zarrouk, R. Salghi, B. Hammouti, M. Elbakri, M. Ebn Touhami, F. Bentiss, H. Oudda, *Res. Chem. Intermed*, (2013) doi: 10.1007/s11164-012-1004-0.
20. M.A. Ameer, E. Khamis, G. Al-Senani, *Adsorpt. Sci. Technol*.18 (2000) 177.
21. E. Khamis, M.A. Ameer, N.M. AlAndis, G. Al-Senani, *Corrosion*. 56 (2000) 127.
22. T. Poornima, J. A. Nayak, N. Shetty, *Corros. Sci.* 53 (2011) 3688.
23. M. Benabdellah, R. Touzani, A. Dafali, B. Hammouti, S. El Kadiri, *Mater. Lett*. 61 (2007) 1197.
24. A.D. Becke, *J. Chem. Phys*. 98 (1993) 5648.
25. D. Frenkel, B. Smit, Understanding Molecular Simulation: From Algorithms to Applications, 2nd Edition, Academic Press: San Diego, (2002).
26. S. Kirkpatrick, C. D. Gelatt, M. P. Vecchi, *Corros. Sci*. 220 (1983) 671.
27. N. Metropolis, A. W. Rosenbluth, M. N. Rosenbluth, A. H. Teller, E. Teller, *J. Chem. Phys*. 21 (1953) 1087.
28. K. F. Khaled, M. N. H. Hamed, K. M. Abdel-Azim, N. S. J. Abdelshafi, *J. Solid. State Electr*.15 (2011) 663.
29. O.L. Jr. Riggs, in: C.C. Nathan (Ed.), Corrosion Inhibitors, second ed., NACE (National Association of Corrosion Engineers), Houston, TX (1973).
30. L. Larabi, Y. Harek, M. Traianel, A. Mansri, *J. Appl. Electrochem*. 34 (2004) 833.
31. F. Mansfeld, M.W. Kendig, S. Tsai, *Corrosion*. 38 (1982) 570.
32. H. Shih, F. Mansfeld *Corros. Sci.* 29 (1989) 1235.

33. S. Martinez, M. Metikoš-Hukovic, *J. Appl. Electrochem*. 33 (2003) 1137.
34. F. Bentiss, M. Lebrini, H. Vezin, F. Chai, M. Traisnel, M. Lagrené, *Corros. Sci*. 51 (2009) 2165.
35. M. Kissi, M. Bouklah, B. Hammouti, M. Benkaddour, *Appl. Surf. Sci*. 252 (2006) 4190.
36. S.F. Mertens, C. Xhoffer, B.C. De Cooman, E. Temmerman, *Corrosion*. 53 (1997) 381.
37. Y.P. Khodyrev, E.S. Batyeva, E.K. Badeeva, E.V. Platova, L. Tiwari, O.G. Sinyashin, *Corros. Sci*. 53 (2011) 976.
38. I.B. Obot, N.O. Obi-Egbedi, *Curr. Appl. Phys*. 11 (2011) 382.
39. W. Chen, H.Q. Luo, N.B. Li, *Corros. Sci*. 53 (2011) 3356.
40. S.S. Abd El-Rehim, M.A.M. Ibrahim, K.F. Khaled, *J. Appl. Electrochem*. 29 (1999) 593.
41. S. Martinez, I. Stern, *Appl. Surf. Sci*. 199 (2002) 83.
42. D. Zhang, Q. Cai, X. M. He, L. X. Gao, G.S. Kim, *Mater. Chem. Phys*. 114 (2009) 612.
43. H. Keles, M. Keles, I. Dehri, O. Serindag, *Mater. Chem. Phys*. 112 (2008) 173.
44. R. Solmaz, E. Altunbas, G. Kardas, *Mater. Chem. Phys*. 125 (2011) 796.
45. G. Avci, *Mater. Chem. Phys*. 112 (2008) 234.
46. E. Bayol, A. A. Gurten, M. Dursun, K. Kayakırılmaz, *Acta Chim. Sinica*. 24 (2008) 2236.
47. O.K .Abiola, N.C. Oforka, *Mater. Chem. Phys*. 83 (2004) 315.
48. M. Ozcan, R. Solmaz, G.Kardas, I. Dehri, *Colloids Surf., A* 325 (2008) 57.
49. F. Hongbo "Synthesis and application of new type inhibitors", Chemical Industry Press, Beijing, (2002) p.166.
50. L. Feng, H. Yang, F. Wang, *Electrochim. Acta*, 58 (2011) 427.